Optical properties of black carbon aerosols encapsulated in a shell of sulfate: comparison of the closed cell model with a coated aggregate model

Research Article | Vol. 25, No. 20 | 2 Oct 2017 | OPTICS EXPRESS 24579
Optics EXPRESS

Optical properties of black carbon aerosols encapsulated in a shell of sulfate: comparison of the closed cell model with a coated aggregate model

MICHAEL KAHNERT[1,2]

[1]*Research Department, Swedish Meteorological and Hydrological Institute, Folkborgsvägen 17, 601 76 Norrköping, Sweden*
[2]*Department of Space, Earth and Environment, Chalmers University of Technology, 412 96 Gothenburg, Sweden*
[*]*michael.kahnert@smhi.se*

Abstract: At 532 nm wavelength, optical properties of black carbon (BC) particles mixed with sulfate are computed by use of two morphological models, a closed cell and a coated aggregate model. For high BC volume fractions f, both models yield comparable results. As more sulfate is added, some of the optical properties diverge. The backscattering depolarization ratio δ_L is particularly sensitive to the morphology. Comparison with field measurements suggests that the closed cell model underestimates δ_L; the coated aggregate model yields good results for intermediate and high values of f, but somewhat too high results for low f. This could be improved by taking the collapse of fractal structure with decreasing f into account.

OCIS codes: (290.5850) Scattering, particles; (010.1100) Aerosol detection; (010.3640) Lidar; (010.1350) Backscattering.

References and links

1. V. Ramanathan and G. Carmichael, "Global and regional climate changes due to black carbon," Nature Geoscience **1**, 221–227 (2008).
2. E. Andersson and M. Kahnert, "Coupling aerosol optics to the MATCH (v5. 5.0) chemical transport model and the SALSA (v1) aerosol microphysics module," Geosci. Model Dev. **9**, 1803–1826 (2016).
3. M. Kahnert, T. Nousiainen, and H. Lindqvist, "Models for integrated and differential scattering optical properties of encapsulated light absorbing carbon aggregates," Opt. Express **21**, 7974–7992 (2013).
4. T. C. Bond and R. W. Bergstrom, "Light absorption by carbonaceous particles: An investigative review," Aerosol Sci. Technol. **40**, 27–67 (2006).
5. M. Hess, P. Koepke, and I. Schult, "Optical properties of aerosols and clouds: The software package OPAC," Bull. Am. Met. Soc. **79**, 831–844 (1998).
6. K. A. Fuller, W. C. Malm, and S. M. Kreidenweis, "Effects of mixing on extinction by carbonaceous particles," J. Geophys. Res. **104**, 15941–15954 (1999).
7. A. Worringen, M. Ebert, T. Trautmann, S. Weinbruch, and G. Helas, "Optical properties of internally mixed ammonium sulfate and soot particles–a study of individual aerosol particles and ambient aerosol populations," Appl. Opt. **47**, 3835–3845 (2008).
8. M. Kahnert, T. Nousiainen, H. Lindqvist, and M. Ebert, "Optical properties of light absorbing carbon aggregates mixed with sulfate: assessment of different model geometries for climate forcing calculations," Opt. Express **20**, 10042–10058 (2012).
9. L. Liu and M. I. Mishchenko, "Scattering and radiative properties of complex soot and soot-containing aggregate particles," J. Quant. Spectrosc. Radiat. Transfer **106**, 262–273 (2007).
10. B. Scarnato, S. Vahidinia, D. T. Richard, and T. W. Kirchstetter, "Effects of internal mixing and aggregate morphology on optical properties of black carbon using a discrete dipole approximation model," Atmos. Chem. Phys. **13**, 5089–5101 (2013).
11. Y. Wu, T. Cheng, L. Zheng, H. Chen, and H. Xu, "Single scattering properties of semi-embedded soot morphologies with intersecting and non-intersecting surfaces of absorbing spheres and non-absorbing host," J. Quant. Spectrosc. Radiat. Transfer **157**, 1–13 (2015).
12. L. Liu, M. I. Mishchenko, and W. P. Arnott, "A study of radiative properties of fractal soot aggregates using the superposition T-matrix method," J. Quant. Spectrosc. Radiat. Transfer **109**, 2656–2663 (2008).
13. M. Kahnert, "On the discrepancy between modelled and measured mass absorption cross sections of light absorbing carbon aerosols," Aerosol Sci. Technol. **44**, 453–460 (2010).

#297019 https://doi.org/10.1364/OE.25.024579
Journal © 2017 Received 7 Jul 2017; revised 15 Sep 2017; accepted 16 Sep 2017; published 27 Sep 2017

Optics EXPRESS

14. M. Kahnert and A. Devasthale, "Black carbon fractal morphology and short-wave radiative impact: a modelling study," Atmos. Chem. Phys. **11**, 11745–11759 (2011).
15. Y. Wu, T. Cheng, L. Zheng, and H. Chen, "Effect of morphology on the optical properties of soot aggregated with spheroidal monomers," J. Quant. Spectrosc. Radiat. Transfer **168**, 158–169 (2016).
16. Y. Wu, T. Cheng, L. Zheng, and H. Chen, "Models for the optical simulations of fractal aggregated soot particles thinly coated with non-absorbing aerosols," J. Quant. Spectrosc. Radiat. Transfer **182**, 1–11 (2016).
17. F. Liu, J. Yon, and A. Bescond, "On the radiative properties of soot aggregates — Part 2: Effects of coating," J. Quant. Spectrosc. Radiat. Transfer **172**, 134–145 (2016).
18. Y. Wu, T. Cheng, L. Zheng, and H. Chen, "Sensitivity of mixing states on optical properties of fresh secondary organic carbon aerosols," J. Quant. Spectrosc. Radiat. Transfer **195**, 147–155 (2017).
19. J. Dong, J. M. Zhao, and L. H. Liu, "Morphological effects on the radiative properties of soot aerosols in different internally mixing states with sulfate," J. Quant. Spectrosc. Radiat. Transfer **165**, 43–55 (2015).
20. K. N. Liou, Y. Takano, and P. Yang, "Light absorption and scattering by aggregates: Application to black carbon and snow grains," J. Quant. Spectrosc. Radiat. Transfer **112**, 1581–1594 (2011).
21. A. R. Jones, "Light scattering in combustion," in "Light Scattering Reviews," A. Kokhanovsky, ed. (2006), Springer, Berlin, pp. 393–444.
22. K. Adachi, S. H. Chung, H. Friedrich, and P. R. Buseck, "Fractal parameters of individual soot particles determined using electron tomography: Implications for optical properties," J. Geophys. Res. **112**, D14202 (2007).
23. D. W. Mackowski, "Calculation of total cross sections of multiple-sphere clusters," J. Opt. Soc. Am. A **11**, 2851–2861 (1994).
24. Y. Wu, T. Cheng, X. Gu, L. Zheng, H. Chen, and H. Xu, "The single scattering properties of soot aggregates with concentric core-shell spherical monomers," J. Quant. Spectrosc. Radiat. Transfer **135**, 9–19 (2014).
25. D. W. Mackowski and M. I. Mishchenko, "A multiple sphere T-matrix Fortran code for use on parallel computer clusters," J. Quant. Spectrosc. Radiat. Transfer **112**, 2182–2192 (2011).
26. D. W. Mackowski and M. I. Mishchenko, "Calculation of the T matrix and the scattering matrix for ensembles of spheres," J. Opt. Soc. Am. A **13**, 2266–2278 (1996).
27. B. T. Draine and P. J. Flatau, "The discrete dipole approximation for periodic targets: theory and tests," J. Opt. Soc. Am. A **25**, 2693–2703 (2008).
28. M. Kahnert, "Numerical solutions of the macroscopic Maxwell equations for scattering by non-spherical particles: A tutorial review," J. Quant. Spectrosc. Radiat. Transfer **178**, 22–37 (2016).
29. A. Lakhtakia and G. W. Mulholland, "On two numerical techniques for light scattering by dielectric agglomerated structures," J. Res. Natl. Inst. Stand. Technol. **98**, 699–716 (1993).
30. M. A. Yurkin and A. G. Hoekstra, "The discrete dipole approximation: An overview and recent developments," J. Quant. Spectrosc. Radiat. Transfer **106**, 558–589 (2007).
31. M. I. Mishchenko, "Light scattering by randomly oriented axially symmetric particles," J. Opt. Soc. Am. A. **8**, 871–882 (1991).
32. N. G. Khlebtsov, "Orientational averaging of light-scattering observables in the T-matrix approach," Appl. Opt. **31**, 5359–5365 (1992).
33. K. Sassen and V. I. Khvorostyanov, "Cloud effects from boreal forest fire smoke: evidence for ice nucleation from polarization lidar data and cloud model simulations," Env. Res. Lett. **3**, 1–12 (2008).
34. S. P. Burton, R. A. Ferrare, C. A. Hostetler, J. W. Hair, R. R. Rodgers, M. D. Obland, C. F. Butler, and A. L. Cook, "Aerosol classification using airborne High Spectral Resolution Lidar measurements — methodology and examples," Atmos Meas. Tech. **5**, 73–98 (2012).
35. T. Murayama, D. Müller, K. Wada, A. Shimizu, M. Sekiguchi, and T. Tsukamoto, "Characterization of Asian dust and Siberian smoke with multiwavelength Raman lidar over Tokyo, Japan in spring 2003," Geophys. Res. Lett. **31**, L23103 (2004).
36. M. Fiebig, A. Petzold, U. Wandinger, M. Wendisch, C. Kiemle, A. Stifter, M. Ebert, T. Rother, and U. Leiterer, "Optical closure for an aerosol column: Method, accuracy, and inferable properties applied to a biomass-burning aerosol and its radiative forcing," J. Geophys. Res. **107**, 8130 (2002).
37. A. Ansmann, M. Tesche, P. Knippertz, E. Bierwirth, D. Althausen, D. Müller, and O. Schulz, "Vertical profiling of convective dust plumes in southern Morocco during SAMUM," Tellus B **61**, 340–353 (2009).
38. N. Sugimoto, B. Tatarov, A. Shimizu, I. Matsui, and T. Nishizawa, "Optical characteristics of forest-fire smoke observed with two-wavelength Mie-scattering lidars and high-spectral-resoluion lidar over Japan," SOLA **6**, 93–96 (2010).
39. S. Groß, M. Esselborn, B. Weinzierl, M. Wirth, A. Fix, and A. Petzold, "Aerosol classification by airborne high spectral resolution lidar observations," Atmos. Chem. Phys **13**, 2487–2505 (2013).
40. A. Nisantzi, R. E. Mamouri, A. Ansmann, and D. Hadjimitsis, "Injection of mineral dust into the free troposphere during fire events observed with polarization lidar at Limassol, Cyprus," Atmos. Chem. Phys. **14**, 12155–12165 (2014).
41. F. Dahlkötter, M. Gysel, D. Sauer, A. Minikin, R. Baumann, P. Seifert, A. Ansmann, M. Fromm, and C. Voigt, "The Pagami Creek smoke plume after long-range transport to the upper troposphere over Europe — aerosol properties and black carbon mixing state," Atmos. Chem. Phys. **14**, 6111–6137 (2014).
42. S. P. Burton, J. W. Hair, M. Kahnert, R. A. Ferrare, C. A. Hostetler, A. L. Cook, D. B. Harper, T. A. Berkoff,

Optics EXPRESS

S. T. Seaman, J. E. Collins, M. A. Fenn, and R. R. Rogers, "Observations of the spectral dependence of particle depolarization ratio of aerosols using NASA Langley airborne High Spectral Resolution Lidar," Atmos. Chem. Phys. **15**, 13453–13473 (2015).
43. M. Kahnert, T. Nousiainen, and H. Lindqvist, "Review: Model particles in atmospheric optics," J. Quant. Spectrosc. Radiat. Transfer **146**, 41–58 (2014).

1. Introduction

The optical properties of black carbon (BC) particles are important for assessing the direct climate forcing effect of BC [1], for the interpretation of Earth observation data sets, or for assimilating remote sensing data into aerosol transport models [2]. The effect of BC on the solar radiative flux, which is relevant for the climate impact of these particles, is mainly determined by the absorption cross section, which can be simulated with sufficient accuracy by use of simple model particles, such as the recently introduced core gray shell model [3]. However, spectral radiometric and polarimetric properties, which are observed with remote sensing techniques, can be significantly more sensitive than broadband radiative net fluxes to the complex morphology and chemical heterogeneity of these particles. Therefore, in order to assess the required level of detail in aerosol optics models it is necessary to assess the impact of morphology on spectral differential scattering properties.

Freshly emitted BC aerosols are fractal aggregates composed of small monomers. As the particles age in the atmosphere the initially lacy structure of the aggregates becomes more compact, the BC material becomes partially oxidized and more hydrophilic, and liquid-phase components, such as sulfate and organic substances can condense onto the particles. As a result, aged BC particles are often covered by a more or less thick liquid film, or they become entirely encapsulated in a nearly spherical shell. At visible wavelengths, this inhomogeneous mixture is characterized by a high optical contrast. While the real and imaginary part of the refractive index of BC is relatively high throughout the short wave part of the spectrum [4], sulfate or organic substances are optically softer and only weakly absorbing at visible wavelengths [5].

Previous studies on BC particles mixed with liquid-phase components have focused on various morphological aspects and their impact on the optical properties. For instance, a non-concentric core-shell model has been employed [6] to study the effect of the BC volume fraction and the relative positioning of the core inside the shell. In another study a model with a spherical sulfate coating containing multiple spherical BC inclusions has been used [7]. Other studies have considered morphologically realistic fractal aggregate models for the BC particle coated by a spherical shell [8], aggregated with a sulfate sphere [9], or partially or fully immersed in a sodium chloride crystal [10]. For semi-embedded fractal aggregates, rather subtle morphological features such as intersecting and non-intersecting surfaces of the aggregate monomers with the sulfate host have been investigated [11]. For bare aggregates, the sensitivity to monomer radius, refractive index, fractal parameters, and monomer size has been investigated in various studies [12–14]. Aggregates composed of spheroidal monomers have also been considered [15]. In [16], both morphologically realistic and simplified models for BC aggregates with a thin coating of organic substances have been compared for BC volume fractions larger than 0.4. In [17] highly realistic BC aggregates with overlapping spheres and "necking" between neighboring spheres have been considered. The coating model was such that the coated BC aggregate remained highly nonspherical regardless of the coating thickness. The sensitivity of optical properties to thin coatings with BC volume fractions larger than 0.8 has been compared to the impact of other particle properties, such as fractal dimension, fractal prefactor, monomer radius, aggregate size, and the refractive index of the coating [18].

Aggregation of BC particles with pure sulfate spheres, such as in the model considered in [9], is unlikely to be common in the atmosphere; encapsulated geometries are more frequently encountered. Therefore, models of BC aggregates encapsulated in a shell of liquid aerosol

Optics EXPRESS

components, as the ones considered in [3, 8, 17], are quite realistic. However, previous models typically employed either a spherical coating (as in [3,8]), or a nonspherical coating (as in [17]). The former is quite realistic for low BC volume fractions, but rather unrealistic for high BC volume fractions; the latter behaves in the opposite way. A larger variety of morphological models, in which different volume fractions and different fractal dimensions were considered simultaneously, has been reported in [19].

It has been proposed to approximate thinly coated aggregates by introducing some simplifying assumptions. Rather than coating the aggregate with a film, one covers each monomer with a concentric shell of coating material; then one builds an aggregate out of these coated monomers [20]. This model has been referred to as the closed cell model; it can be hypothesized to represent the optical properties of coated BC particles with sufficient accuracy provided that the BC volume fraction is high. But it is unlikely to work well for low BC volume fractions.

The study presented in this paper aims at devising a model with the potential to cover the whole range of BC volume fractions. In this model the BC aggregate is coated with a thin film at high BC volume fractions. As more coating material is added and the BC volume fraction decreases, the coating becomes more and more spherical. The optical properties obtained with this model are compared to those computed with the closed cell model. Model uncertainties are estimated by computing optical properties for different stochastic realizations of the fractal aggregate geometries, and by computing ensemble-averages and maximum variations around the mean value. This allows one to decide in which cases the differences between the two models are significant.

Many previous studies on the optical properties of BC aerosols had a strong focus on the radiative forcing effect of black carbon. For this reason, several publications focus almost exclusively on climate-relevant optical properties, such as the absorption and scattering cross sections, the single scattering albedo, and the asymmetry parameter (e.g. [18, 19]). The present study is mostly designed with remote sensing and inverse modeling applications in mind. Therefore, much emphasis will be placed on the phase function, on the backscattering cross section, and on the linear backscattering depolarization ratio, as well as on estimating the forward model error introduced by uncertainties in the particle geometry.

The model particles and computational methods are introduced in Sec. 2. Computational results are presented and discussed in Secs. 3 and 4, respectively. Concluding remarks are given in Sec. 5.

2. Methods

All optical properties are computed at a visible wavelength of 532 nm.

2.1. Model particles

The BC model particles are assumed to be fractal aggregates composed of N_s spherical monomers of constant radius a, where the fractal geometry is characterized by the scaling relation [21]

$$N_s = k_0 \left(\frac{R_g}{a} \right)^{D_f} . \tag{1}$$

Here D_f and k_0 are the fractal dimension and fractal prefactor, respectively, and the radius of gyration

$$R_g = \sqrt{\frac{1}{N_s} \sum_{i=1}^{N_s} | \vec{r}_i - \vec{r}_c |^2} \tag{2}$$

Optics EXPRESS

expresses the geometric mean of the distances of the monomer positions $\vec{r}_i$ from the aggregate's center of mass $\vec{r}_c$. The model particles used in this study are characterized by the parameters a=25 nm, D_f=2.4, and k_0=0.7, which are based on mean values obtained by 3D electron tomography measurements on field samples of aged soot particles [22]. Four aggregate sizes are considered, namely, N_s=8, 64, 216, and 512. For each aggregate size, ten stochastic realizations of the geometry characterized by the same fractal parameters were generated by use of the cluster aggregation algorithm developed in [23]. The bare aggregates were then coated with sulfate. For the BC volume fraction $f = V_{\mathrm{BC}}/V_{\mathrm{total}}$ five different values were considered, namely, f=10, 25, 50, 75, and 100 %, where the last value represents bare BC aggregates.

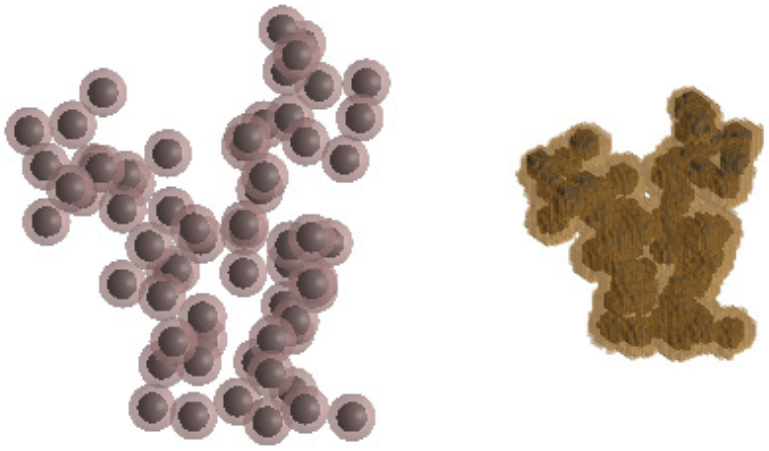

Fig. 1. Closed cell (left) and coated aggregate model (right) for black carbon aerosol particles mixed with sulfate. Both particles are composed of 64 monomers, and the total volume, the BC volume fraction, and the relative positioning of the monomers are identical in both cases.

Two different models are considered for representing coated aggregates, which are illustrated in Fig. 1.

1. **Closed cell model:** In this model, each individual BC monomer is coated by a concentric spherical shell of sulfate of radius a_c, which is related to the BC monomer radius a such that $a^3/a_c^3 = f$. The relative positioning of the monomers in the closed cell model is exactly as in the original bare aggregate. However, in the bare aggregate the neighboring BC monomers are in point contact with each other, while in the closed cell model the sulfate coatings of neighboring coated monomers are in point contact. The left panel in Fig. 1 shows an example for $N_s = 64$ monomers and a BC volume fraction of 25 %. This model has been applied in earlier studies on coated BC aerosols (e.g. [20, 24]). The term "closed cell model" has been used specifically in [20].

2. **Coated aggregate model:** Rather than coating each individual monomer with a sulfate shell prior to aggregating the monomers, in this model the BC monomers are aggregated first; then the coating is added. The right panel in Fig. 1 shows an example for $N_s = 64$ monomers and a BC volume fraction of 25 %. The relative positioning of the monomers, and thereby the fractal parameters, are exactly the same in the two particles shown in Fig. 1.

   The coating is done by the following algorithm adapted to be used in conjunction with the discrete dipole approximation (DDA, see next section). In the DDA the volume of the

Optics EXPRESS

target particle is discretized into small volume cells of length d, and in each volume cell occupied by the particle the material's refractive index is specified. Suppose the maximum dimension of the aggregate is D (see Fig. 2, left). Then we take the smallest circumscribing sphere (the diameter of which is D), and we increase its diameter to $D_C = D + 2d$ while keeping the center of the sphere fixed. Thus the distance from the outermost points of the aggregate to the surface of the circumscribing sphere is equal to d. We then add successive "onion rings" of sulfate onto the aggregate. These layers have thickness d and are constrained to lie within the circumscribing sphere. This is illustrated schematically in Fig. 2, right panel. The coating material is added until either the desired BC volume fraction f is reached, or until the circumscribing sphere is completely filled with coating material. If the latter is the case, then we proceed by adding spherical layers of sulfate onto the circumscribing sphere until we reach the prescribed volume fraction f. Thus the particle grows increasingly more spherical during the coating process.

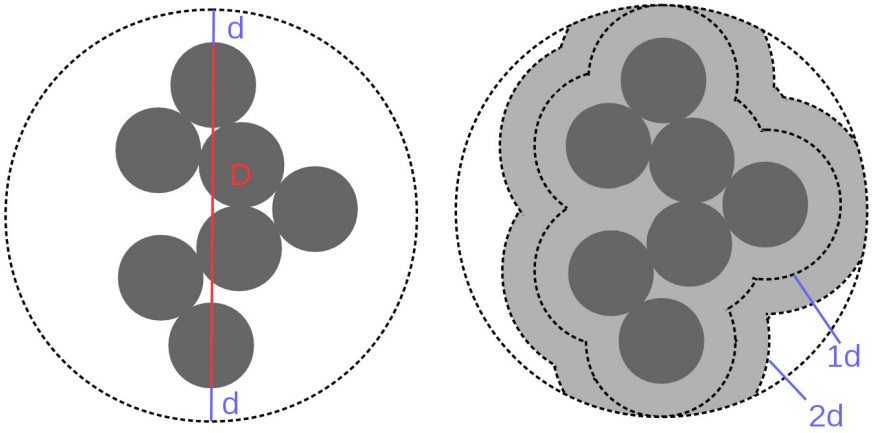

Fig. 2. Principle of the coated aggregate model. Left: BC aggregate with circumscribing sphere of diameter $D_C = D + 2d$. Right: Coating of thickness $1d$ and $2d$, each constrained to lie inside the circumscribing sphere.

To implement this model efficiently, one first determines the BC volume fraction f_C of a particle in which the circumscribing sphere is completely filled. If $f_C > f$, then we need to add more sulfate than the amount contained in the circumscribing sphere. In that case we simply compute the diameter of the sphere that yields the correct volume fraction f (which will be larger than D_C) and fill all volume cells inside that sphere with sulfate, unless they are already occupied by BC. The overall shape of the particle will be spherical, but it will contain a nonspherical BC aggregate inside. If, on the other hand, $f_C < f$, then the circumscribing sphere should not be completely filled with sulfate. In that case we determine, for each volume cell inside the circumscribing sphere, its minimum distance to the BC aggregate. Then we coat the aggregate successively, i.e., we first fill all volume cells with sulfate that have a minimum distance to the aggregate of d; next we fill those cells inside the circumscribing sphere with a minimum distance of $2d$, then $3d$, etc, until the number of sulfate-occupied volume cells N_{SO4} is such that $f = N_{BC}/(N_{BC} + N_{SO4})$, where N_{BC} is the number of volume cells occupied by BC. For high BC volume fractions, this algorithm produces coated aggregates with shapes that are very close to the bare aggregate shape, while for low BC volume fractions, the shapes become more and more spherical. We assume that this mimics, at least qualitatively, the behavior of real particles that grow by condensation processes of sulfate onto BC

Optics EXPRESS

aggregates.

For high BC volume fractions (i.e., small amount of sulfate), the geometries generated with this model are similar to those in [16–18]. However, as the amount of coating is increased, those models tend to produce highly nonspherical particles with overall shapes that strongly resemble the original aggregate (see, e.g., the rightmost particles in Fig. 2 in [17]). By contrast, the model devised here takes into account that the coating has a tendency to become increasingly more spherical as the amount of coating material is increased.

2.2. Computational methods

The optical properties of closed cell particles are computed with the superposition T-matrix method, which is implemented in the publicly available T-matrix code MSTM Version 3.0 [25]. This method is applicable to particles composed of multiple spheres with the restriction that the surface of any two spheres must not overlap. In the T-matrix formulation of the light scattering problem orientation averaged optical properties can be derived as closed form expressions of the T-matrix, which allows for very efficient and accurate numerical computations [26]. A detailed introduction into the superposition T-matrix method is given in [23, 25].

The optical properties of the coated aggregates are computed with the discrete dipole approximation (DDA). This is a volume integral equation method for solving the light scattering problem, in which the particle volume is discretized into volume cells much smaller than the wavelength in the dielectric medium. By assuming that the field is nearly constant in each volume cell, one effectively represents each volume cell by a single dipole. The polarizability of each dipole is being related to the refractive index in each volume cell by use of a suitable polarizability model. This approach allows one to convert the volume integral equation into an algebraic equation that can be solved with standard numerical techniques. We used the publicly available DDA code DDSCAT Version 7.1 [27].

A great advantage of the method is that it can be applied to arbitrary particle morphologies. A drawback is that orientation averaged optical properties have to be computed by numerical orientation averaging. Both the volume cell size (or dipole distance d) and the number of discrete orientation angles need to be determined carefully in order to ensure the accuracy of the computational results. A very brief introduction to the theory can be found in [28]. More detailed introductions into the DDA theory are found in [29, 30].

2.3. Computational aspects

There are two important aspects regarding the accuracy of the DDA computations. First we have to determine how many discrete angles we need to employ in the numerical averaging over random particle orientations. Second, we need to determine the minimum required dipole spacing d.

As a reference one can employ T-matrix computations for bare black carbon aggregates. Figure 3 shows the elements of the Stokes scattering matrix of a black carbon aggregate consisting of 64 monomers, computed with the MSTM T-matrix code (black line, left column). These results are based on the analytic orientation-averaging procedure in the T-matrix approach [31, 32]. Corresponding DDA results in Fig. 3 (red line, left column) have been obtained by averaging over 864 discrete orientational angles, and by using a dipole spacing d such that $|m|kd=0.14$, where k is the wavenumber of light, and where m is the complex refractive index of black carbon. Evidently this number of discrete angles is sufficient for reproducing the T-matrix reference results with high accuracy.

The right column in Fig. 3 shows the difference between the DDA and the T-matrix results, where the DDA computations were performed by averaging over 864 discrete angles, and where the dipole spacing d in the DDA method has been varied such that $|m|kd=0.14$ (red line),

Optics EXPRESS

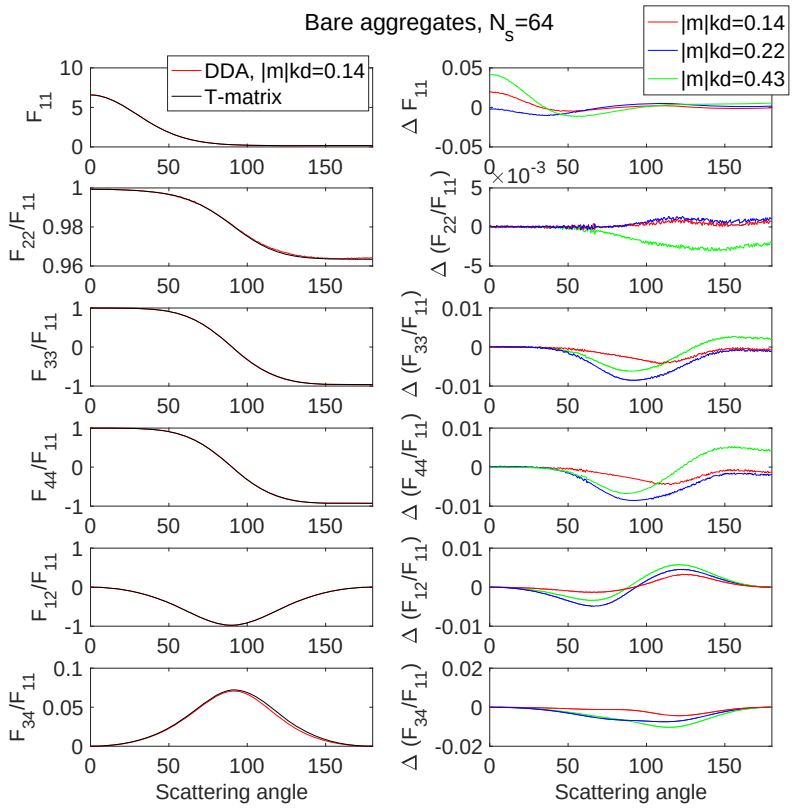

Fig. 3. Left column: Elements of the Stokes scattering matrix of bare BC aggregates composed of 64 monomers, computed with the superposition T-matrix method and analytic orientation averaging (black, reference case), and with the discrete dipole approximation (red), using a dipole spacing d with $|m|kd$=0.14 and 864 discrete orientation angles. Right: Differences between the DDA and the reference T-matrix results for $|m|kd$=0.14 (red), 0.22 (blue), and 0.43 (green).

0.22 (black line), and 0.43 (green line). Clearly, the DDA results converge toward the T-matrix results as the dipole spacing is decreased.

What accuracy do we need for our purposes? We will focus on the element F_{22}/F_{11} of the Stokes scattering matrix in the backscattering direction, as this quantity is particularly sensitive to both particle shape and to the dipole spacing. Figure 4 shows F_{22}/F_{11} computed with the T-matrix approach for a bare BC aggregate with N_s=64 monomers, and for 10 stochastic realizations of the geometry with the same fractal parameters. In the backscattering direction the span from the smallest value (0.961) to the largest value (0.984) in the ensemble is about 0.023. This should be compared to $\Delta(F_{22}/F_{11})$ in Fig. 3 (second row right). For the coarsest dipole spacing of $|m|kd$=0.43, we obtain $\Delta(F_{22}/F_{11})$=0.002, which is one order of magnitude smaller than the variation among different stochastic geometries in Fig. 4. We can also compute the linear backscattering depolarization ratio

$$\delta_L = \left.\frac{F_{11} - F_{22}}{F_{11} + F_{22}}\right|_{\Theta=180^\circ}, \tag{3}$$

where the elements of the Stokes scattering matrix are taken in the backscattering direction,

Optics EXPRESS

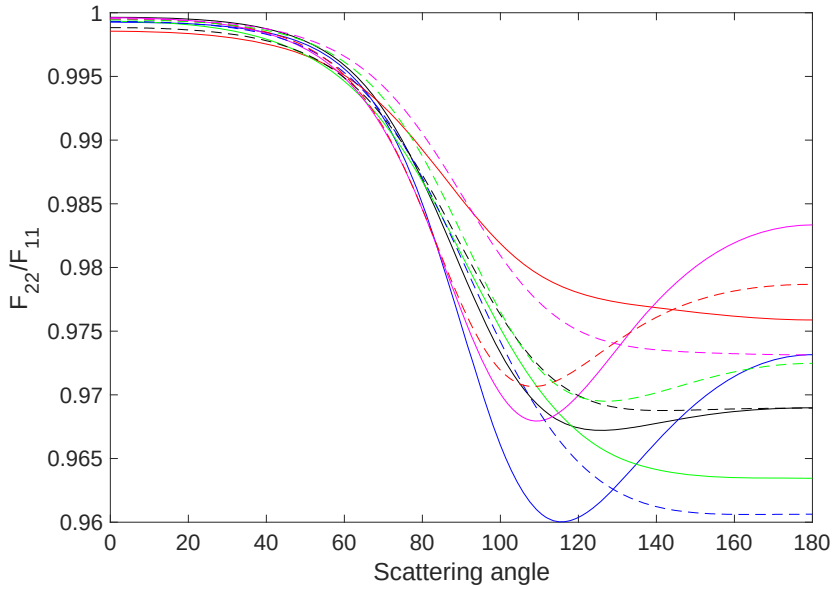

Fig. 4. Element F_{22}/F_{11} of the Stokes scattering matrix computed with the superposition T-matrix method for 10 stochastic realizations of a fractal aggregate with prescribed fractal parameters consisting of 64 monomers.

i.e., at a scattering angle $\Theta = 180°$. The span of δ_L values obtained for the 10 stochastic realizations of the aggregate geometry is 0.021. For a dipole spacing of $|m|kd$=0.43 the DDA computations yield δ_L values that are slightly lower than the T-matrix reference results by an amount of 0.001, which, again, is more than an order of magnitude smaller than the range of uncertainty related to the variability in geometry. We can conclude that a dipole spacing of $|m|kd$=0.43 will be sufficient for our purposes.

3. Results

We now turn to comparing T-matrix results for the closed cell model to DDA results for the coated aggregate model. Figure 5 presents results obtained for these two models, namely, the total scattering cross section C_{sca} (first column), the absorption cross section C_{abs} (second column), the backscattering cross section C_{bak} (third column), and the linear backscattering depolarization ratio δ_L (fourth column). The results in Fig. 5 are presented as a function of the volume-equivalent particle radius R_V. The rows of the plot pertain to different BC volume fractions f, namely, 100 % (i.e., bare aggregates, first row), 75 % (second row), 50 % (third row), 25 % (fourth row), and 10 % (fifth row). Note that the scale of R_V is different in each row, since the amount of sulfate coating increases from top to bottom as the BC volume fraction is decreased. For each aggregate size, computations were performed for 10 stochastic realizations of an aggregate with prescribed fractal parameters. The lines in the figure represent the ensemble averages, while the shaded regions indicate the maximum variation within the 10-particle ensemble. The red lines indicate DDA results obtained for the coated aggregate model, the blue lines represent MSTM results for the closed cell model.

The first important observation is that the cross sections, including C_{bak}, display virtually no variation among the 10 stochastic geometries, not even for the largest particle sizes. By contrast, δ_L can vary considerably among different geometries. This is consistent with results reported

Optics EXPRESS

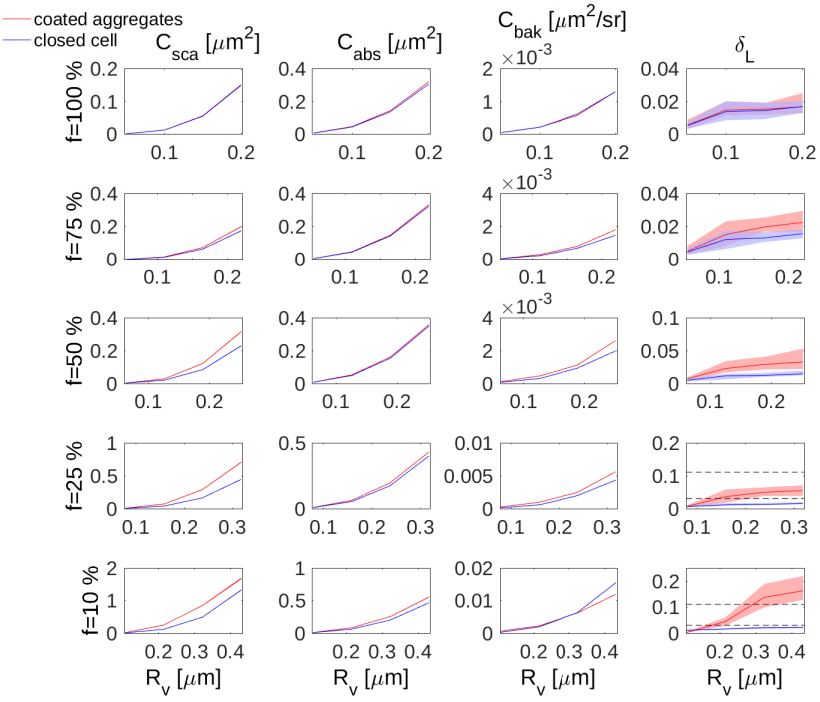

Fig. 5. Total scattering cross section (first column), absorption cross section (second column), backscattering cross section (third column), and linear backscattering depolarization ratio (fourth column) for BC volume fractions f =100 % (first row), 75 % (second row), 50 % (third row), 25 % (fourth row), and 10 % (fifth row), each computed for coated aggregates (red) and closed cells (blue). The optical properties are shown as a function of the volume-equivalent particle radius. For an ensemble consisting of ten stochastic realizations of the aggregate geometry the arithmetic ensemble-mean and the maximum variation are represented by the solid lines and the shadings, respectively. Dashed lines (rightmost panels in rows 4 and 5) indicate a range of typical field observations.

in [8]. This indicates that aggregates with different geometries but with equal fractal parameters form, as far as the cross sections are concerned, an "optical equivalence class". But this is not so with regard to δ_L. To obtain a meaningful estimate of this quantity it is necessary to compute an ensemble-average over several stochastic realizations of the aggregate geometry.

The second observation in Fig. 5 is that there are rather moderate differences in the optical cross sections computed with the coated aggregate and the closed cell model. The differences generally increase with increasing volume-equivalent particle radius R_V and with decreasing BC volume fraction f. Both models agree, as they should, for f=100 % (i.e., for bare aggregates). The more sulfate is added to the aggregates, the more the scattering cross sections differ between the two models. This effect is much less pronounced for the absorption cross section, for which both models agree quite well for BC volume fractions as low as 25 %. The backscattering cross sections agree reasonably well for particle radii up to about 150–200 nm, beyond which the two models start to diverge even for BC volume fractions as high as 75 %. But generally, the discrepancies in the cross sections seem to be less pronounced than those observed for the linear backscattering depolarization ratio δ_L. For f =75 %, the two models agree within their respective ranges of variability (second row right). For $f \leq 50$ % the differences between the two models are larger than the variations within the ensemble of geometries (third through fifth

Optics EXPRESS

row right). These differences generally increase with increasing particle radius and decreasing BC volume fraction.

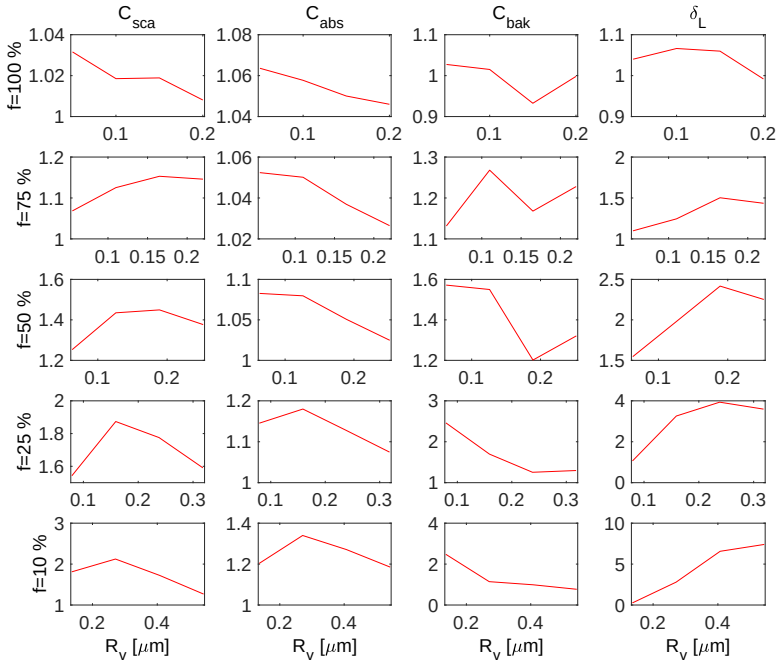

Fig. 6. Ratios of the mean optical properties computed with coated aggregates to those computed with the closed cell model. The rows and columns are as in Fig. 5.

Figure 6 shows the ratio of each of the optical properties in Fig. 5 computed with the coated aggregate model to that computed with the closed cell model. One can see that the scattering cross section in the coated aggregate model does exceed that computed with the closed cell model by as much as a factor of two, but only in some isolated cases, and only for smaller particles. For larger particles, which have the largest cross sections, the relative differences, are generally less than a factor of two, even for the lowest BC volume fractions. For the absorption cross sections, the ratio between the two models rarely exceeds a factor of 1.15. Even for the backscattering cross section, the ratio exceeds a factor of 1.5 only for small particle radii, for which the magnitude of C_{bak} is small. The corresponding ratio of δ_L is less than 1.5 for a BC volume fraction of f=75 %, and it increases to 2.5, 4, and 7.5 at f=50, 25, and 10 %, respectively. This clearly illustrates that δ_L is most sensitive to the choice of particle model.

In Fig. 7 we compare the phase functions F_{11} computed with the two particle models. The columns show results for different aggregate sizes, namely, for N_s=8 (first column), 64 (second column), 216 (third column) and 512 monomers (fourth column). For each of these aggregate sizes, the rows show results for different volume fractions, namely, f=100 % (pure aggregates, first row), 75 % (second row), 50 % (third row), 25 % (fourth row), and 10 % (fifth row). As in Fig. 5, the lines show the ensemble-average over the ten geometries. The maximum variation is also indicated; but it is so small that it can hardly be discerned.

In all cases, the differences seem to be rather small; however, note that the phase functions are plotted on a logarithmic scale. For instance for N_s=512 and f=10 % (bottom right), the phase function in the forward-scattering direction computed with the closed cell model (red line) is larger by almost a factor of 3 than that computed with the coated aggregate model (blue line).

Optics EXPRESS

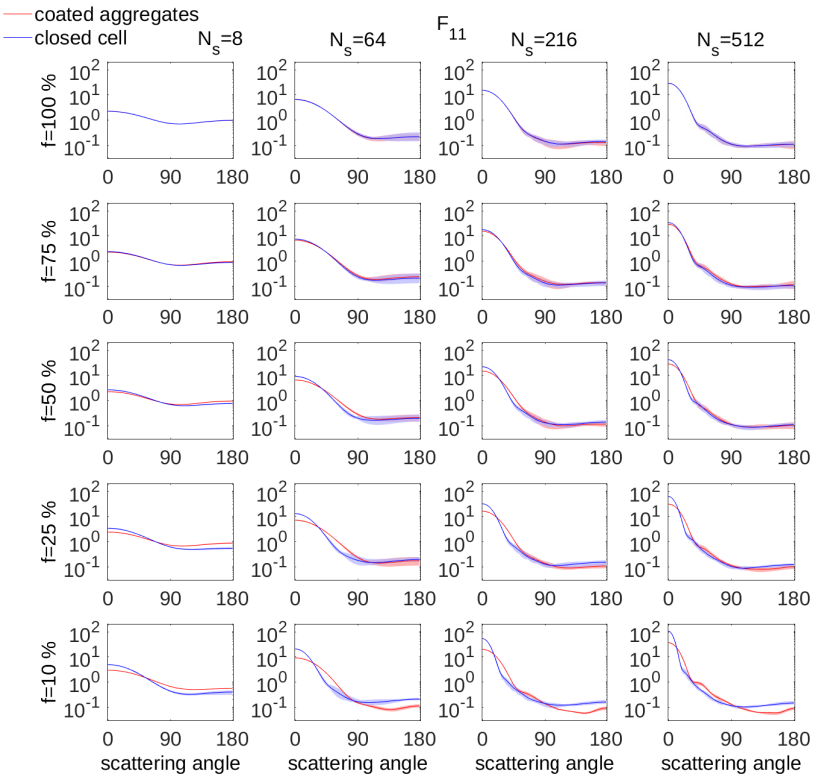

Fig. 7. Element F_{11} of the Stokes scattering matrix computed for aggregate sizes of N_s =8 (first column), 64 (second column), 216 (third column), and 512 (fourth column). The rows and colors are as in Fig. 5.

In general, the coated aggregate model gives broader forward-diffraction peaks and lower phase function values in the backscattering direction than the closed cell model.

In Fig. 8 we compare the element F_{22}/F_{11} for the two particle models. The rows, columns, and colors are as in Fig. 7. The coated aggregate model consistently predicts lower values than the closed cell model, especially in the backscattering direction. The differences strongly increase with decreasing BC volume fraction (from top to bottom); they also increase with aggregate size (from left to right). This agrees with the observations in Fig. 5, which demonstrated that the coated aggregate model predicts larger linear backscattering depolarization ratios δ_L than the closed cell model.

4. Discussion

In comparison to real-world encapsulated BC aggregates, the coated aggregate model is, arguably, morphologically more realistic than the closed cell model. However, that alone does not guarantee that it will provide more accurate estimates of the optical properties. For this reason, I have deliberately refrained in the previous section from using the coated aggregate model as a reference, and from judging the closed cell model by how well it agrees with that reference. All we can say, so far, is that there are cases in which both models differ substantially in the differential scattering properties. This is particularly pronounced for δ_L and F_{22}/F_{11}.

An evaluation of both models that goes beyond a mere comparison can only be based on

Optics EXPRESS

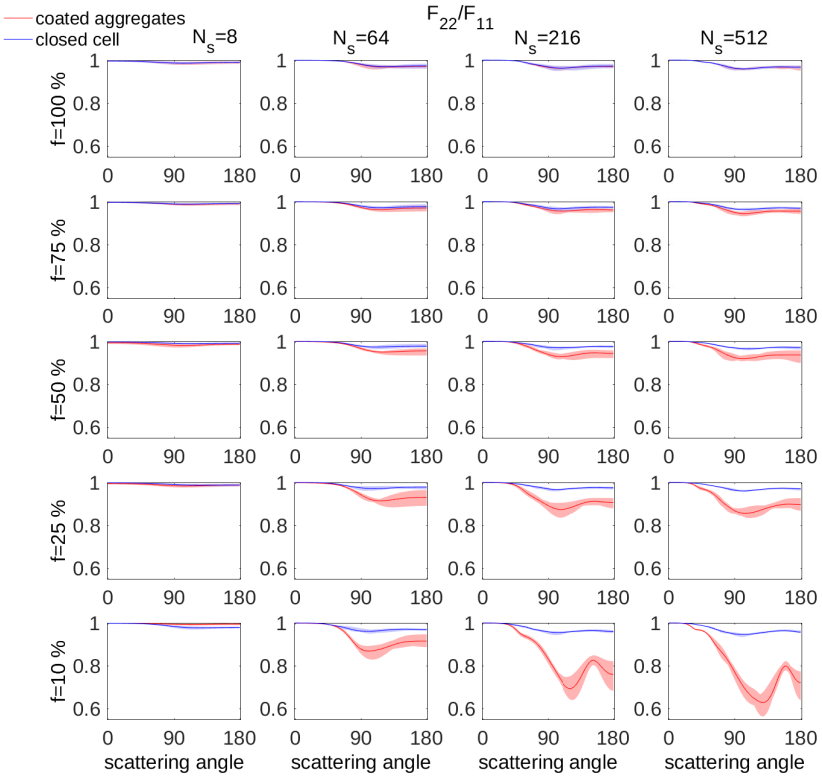

Fig. 8. Element F_{22}/F_{11} of the Stokes scattering matrix. The columns, rows and colors are as in Fig. 6.

information from measurements. Table 1 lists δ_L values measured in various field campaigns by use of either ground-based or airborne lidar instruments at 532 nm. In two cases one was observing fresh BC aerosols originating from nearby sources. The corresponding δ_L values were $<$ 3 % in one case [33], and 2–5 % in the other [34]. Fresh BC can be expected to have a high BC volume fraction. In the computations reported here, particles with high volume fractions have relatively low depolarization ratios in either model. For instance, for particles with f $\leq$50 %, the closed cell model predicts δ_L to lie in the range 0.3–2 %. Corresponding results for the coated aggregate model lie in the range 0.3–3 %. Either is consistent with the observations in [33, 34].

Two cases in table 1 stick out, namely, the Mongolian fire case [38] with δ_L in the range 12–15, and the Turkish fire case [40] with δ_L in the range 9–18. In either case the smoke plumes were contaminated with dust, which explains the relatively high depolarizations. If we disregard these two cases as well as the two observations of fresh BC, then the remaining observations of aged smoke plumes give δ_L values in the range 3–11 %. This range is indicated by dashed lines in Fig. 5 (rightmost panels in rows 4 and 5). Aged BC can be expected to have a relatively low BC volume fraction. For instance, for a BC volume fraction of f=10 % the depolarization ratio δ_L computed with the coated aggregate model lies in the range 4–13 % for sizes in the range of 200–300 nm, which is consistent with the observations. However, for large particles with a volume-equivalent radius of around 450 nm, δ_L can be as high as 16 %, which is higher than the values that are typically observed in the field. Corresponding results obtained with the

Optics EXPRESS

Table 1. Linear backscattering depolarization ratio δ_L from various field measurements.

δ_L (%)	Source	Type of BC	Location of observation	Ref.
6	Siberian smoke	aged	Tokyo, Japan	[35]
6–11	Canadian smoke	aged	LACE, Germany	[36]
< 3	Alaskan smoke (local)	fresh	Fairbanks, Alaska	[33]
5	Alaskan aged (regional)	aged	Fairbanks, Alaska	[33]
4–5	African biomass burning	aged	Manaus, Brazil	[37]
12–15	Mongolian forest fire	aged + dust	Nagasaki and Tsukuba, Japan	[38]
2–5	North American smoke	fresh	North America, various flight campaigns	[34]
3–8	Siberian smoke	aged	North America, various flight campaigns	[34]
5–9	Canadian forest fire	aged	LACE, Central Europe	[39]
9–18	Turkish fires	aged + dust	Limassol, Cyprus	[40]
6–8	North American smoke	aged	Germany	[41]
6–9	Pacific NW, North America	aged	Colorado, North America	[42]

closed cell model lie in the range 1–3 %. Thus the closed cell model cannot explain δ_L values exceeding 4 %, which applies to the majority of the observations of aged BC listed in Table 1.

This comparison needs to be taken with a grain of salt. We lack information about the fractal parameters, monomer radii, aggregate sizes, volume fractions, and the chemical composition of the coating in the smoke plumes observed in field measurements. Also, it is not trivial to decide whether or not observed smoke plumes may be contaminated by other types of aerosols. Equally important, the estimate of our model uncertainties is based on stochastic variations in the fractal geometry only. Other sources of error are not accounted for, such as uncertainties in the refractive index of BC and the coating, uncertainties in fractal parameters, monomer radii, and in subtle morphological features, such as nonspherical or overlapping monomers or "necking" among neighboring monomers. Thus the comparison of the modeling results with the measurements in table 1 constitutes by no means a validation of the model. What we can conclude is that the coated aggregate model covers a larger range of depolarization values than the closed cell model. But there does seem to be a risk that the coated aggregate model overestimates depolarization by large particles with low BC volume fractions. A possible reason may be that in this model the coating tends to have an overall nonspherical shape even for low BC volume fractions, because the BC aggregate is always fully encapsulated in the shell. By contrast, the encapsulated aggregate model considered by [8] was based on the assumption that the coating is always perfectly spherical, while part of the aggregate was allowed to stick out of the coating (see Figure 1 in that paper). For a BC volume fraction of 7 % and a wavelength of 533.2 nm, δ_L did not exceed 10 %, not even for particles with volume-equivalent radii of 500 nm (see Figure 5 in that paper). This is well within the range of observed depolarization ratios of aged BC aggregates listed in Table 1. However, a perfectly spherical coating becomes increasingly unrealistic as the BC volume fraction is increased. In such case, the coated aggregate model considered here, in which the coating follows the aggregate shape, is morphologically more realistic than that in which the coating has perfect spherical shape.

Another significant omission in the coated aggregate model as defined here was that the fractal dimension has been kept constant. In reality, the fractal aggregate will increasingly collapse and become more compact as it ages and as more coating material is added. As a result, the overall shape of real coated aggregates is likely to be somewhat more spherical than that in the model. In future studies one should test the effect of introducing either or both of the following modifications.

1. Increase the fractal dimension with decreasing BC volume fraction.

Optics EXPRESS

2. Decrease the diameter D_C of the sphere that defines the onset of sphericity of the coating.

Either of these changes is likely to reduce the depolarization ratio of the model particles at low BC volume fractions.

5. Summary and conclusions

This study was based on the hypothesis that the closed cell model and the coated aggregate model should give similar results for high BC volume fractions, and that they should increasingly diverge as the BC volume fraction is lowered, i.e., as more sulfate is added to the BC aggregate. To a large extent, the computational results confirm this hypothesis.

At a wavelength of 532 nm field observations with lidar instruments have detected depolarization ratios of aged smoke particles in the range of 3–11 %. The closed cell model predicts depolarization ratios that are lower than those obtained in field observations. For intermediate volume fractions and intermediate particle sizes the coated aggregate model produces depolarization ratios that lie within the range of typical field observations. However, this model may produce somewhat too high δ_L values for very low BC volume fractions and large particle sizes. This could probably be improved by introducing some modifications to the model considered here, namely by (i) increasing the fractal dimension of the BC core with decreasing BC volume fraction; and/or (ii) reducing the diameter D_C of the sphere that defines the boundary between spherical and nonspherical coatings.

The analysis of the results allows us to formulate a more detailed hypothesis. While the closed cell model appears to be sufficiently accurate for high BC volume fractions, the coated aggregate model considered here is a promising candidate for computing δ_L for intermediate BC volume fractions and particle sizes, and the model considered in [8] appears to be most suitable for low BC volume fractions and large particle radii. However, with appropriate modifications, the coated aggregate model may be capable of producing accurate estimates of the optical properties over the entire range of BC volume fractions. More dedicated measurements under controlled laboratory condition are necessary to subject this hypothesis to further scrutiny.

Finally, it has to be stressed that it is not a model's sole purpose to fit measurements. In many modeling studies the aim is to gain physical insight into the light-scattering process. This can often be easier to achieve by using models of somewhat reduced morphological complexity. (For a more detailed discussion of this point see the review in [43]). Thus the usefulness of the coated aggregate and closed cell models must not exclusively be judged by its ability to reproduce observations.

Funding

Swedish Research Council (*Vetenskapsrådet*) (2016-03499).

Acknowledgments

Dan Mackowski and Michael Mishchenko are gratefully acknowledged for making the MSTM code publicly available. I am further indebted to Dan Mackowski for making his cluster aggregation program available. Finally, I am grateful to Bruce Draine and Pjotr Flatau for making the DDSCAT program publicly available.